

Reliable Prediction with Tuned Range-Separated Functionals of the Singlet-Triplet Gap in Organic Emitters for Thermally Activated Delayed Fluorescence (TADF)

Haitao Sun, Cheng Zhong, and Jean-Luc Bredas

J. Chem. Theory Comput., **Just Accepted Manuscript** • DOI: 10.1021/acs.jctc.5b00431 • Publication Date (Web): 09 Jul 2015

Downloaded from <http://pubs.acs.org> on July 12, 2015

Just Accepted

“Just Accepted” manuscripts have been peer-reviewed and accepted for publication. They are posted online prior to technical editing, formatting for publication and author proofing. The American Chemical Society provides “Just Accepted” as a free service to the research community to expedite the dissemination of scientific material as soon as possible after acceptance. “Just Accepted” manuscripts appear in full in PDF format accompanied by an HTML abstract. “Just Accepted” manuscripts have been fully peer reviewed, but should not be considered the official version of record. They are accessible to all readers and citable by the Digital Object Identifier (DOI®). “Just Accepted” is an optional service offered to authors. Therefore, the “Just Accepted” Web site may not include all articles that will be published in the journal. After a manuscript is technically edited and formatted, it will be removed from the “Just Accepted” Web site and published as an ASAP article. Note that technical editing may introduce minor changes to the manuscript text and/or graphics which could affect content, and all legal disclaimers and ethical guidelines that apply to the journal pertain. ACS cannot be held responsible for errors or consequences arising from the use of information contained in these “Just Accepted” manuscripts.



1
2
3 **Reliable Prediction with Tuned Range-Separated Functionals of the**
4
5 **Singlet-Triplet Gap in Organic Emitters**
6
7 **for Thermally Activated Delayed Fluorescence (TADF)**
8
9

10
11
12
13 **Haitao Sun, Cheng Zhong, and Jean-Luc Brédas***
14
15

16
17
18 *Physical Science and Engineering Division*

19 *Solar & Photovoltaics Engineering Research Center*

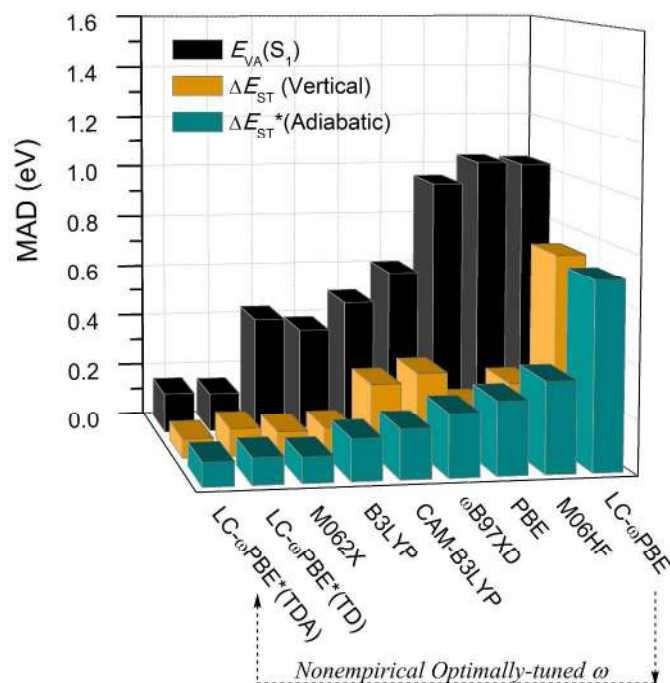
20 *King Abdullah University of Science and Technology (KAUST)*

21 *Thuwal 23955-6900, Kingdom of Saudi Arabia*
22
23
24
25
26
27
28
29
30
31
32
33
34
35
36
37
38
39
40
41
42
43
44
45
46
47
48
49
50
51

52 Corresponding author: jean-luc.bredas@kaust.edu.sa
53
54
55
56
57
58
59
60

Abstract

The thermally activated delayed fluorescence (TADF) mechanism has recently attracted much interest in the field of organic light-emitting diodes (OLEDs). TADF relies on the presence of a very small energy gap between the lowest singlet and triplet excited states. Here, we demonstrate that time-dependent density functional theory (TD-DFT) in the Tamm-Dancoff Approximation can be very successful in the calculations of the lowest singlet and triplet excitation energies and the corresponding singlet-triplet gap when using nonempirically tuned range-separated functionals. Such functionals provide very good estimates in a series of 17 molecules used in TADF-based OLED devices, with mean absolute deviations of 0.15 eV for the vertical singlet excitation energies and 0.09 eV [0.07 eV] for the adiabatic [vertical] singlet-triplet energy gaps as well as low relative errors and high correlation coefficients compared to the corresponding experimental values. They significantly outperform conventional functionals, a feature which is rationalized on the basis of the amount of exact-exchange included and the delocalization error. The present work provides a reliable theoretical tool for the prediction and development of novel TADF-based materials with low singlet-triplet energetic splittings.



1. Introduction

Organic π -conjugated molecules substituted by appropriate donor and acceptor groups (D/A) are known to exhibit interesting optoelectronic properties¹ due to their significant charge-transfer (CT) characteristics upon photoexcitation. Such compounds have attracted considerable attention in particular in the fields of organic nonlinear optics,² organic field-effect transistors,³ and organic photovoltaic cells.^{4,5} Recently, donor-acceptor structural arrangements have also been key in the development of thermally activated delayed fluorescence (TADF)⁶⁻¹⁰ materials, which represent the third generation of organic light-emitting diodes (OLEDs).¹¹

In OLEDs, electrons injected from a cathode and holes injected from an anode recombine into luminescent molecules in the active layer and bring them in their excited states. When spin statistics is obeyed, this process leads 75% of the time to formation of a triplet excited state and 25% of the time to a singlet excited state. In the case of purely organic molecules, the triplet excited state is dark and the maximum internal quantum efficiency is then limited to 25%. However, when the energy gap (ΔE_{ST}) between the lowest singlet (S_1) and triplet (T_1) excited states is small enough, up-conversion from T_1 to S_1 can take place under assistance of thermal energy. Ideally, all of the triplet excitons (75%) should be able to convert into S_1 and fluoresce, which can lead to an internal quantum efficiency close to 100% (Figure 1).¹² Adachi and co-workers have demonstrated that a very small ΔE_{ST} is essential, although not sufficient, to achieve efficient TADF via such a $T_1 \rightarrow S_1$ reverse intersystem crossing (ISC).^{6,13} A small ΔE_{ST} can

1
2
3 usually result from spatial separation between the highest occupied molecular orbital (HOMO)
4
5 and the lowest unoccupied molecular orbital (LUMO).¹⁴
6
7

8
9
10 Despite their potential usefulness in this emerging field, theoretical investigations of the excited
11
12 states and excitation spectra of TADF-based materials remain relatively limited and have proven
13
14 to be challenging. A main issue from a theoretical perspective is to find the appropriate level of
15
16 theory capable of providing both efficient (qualitative) and accurate (quantitative) predictions of
17
18 the electronic structures of large charge-transfer-type molecules.¹⁵ Indeed, TADF molecules
19
20 often consist of > 100 atoms, which limits their studies with high-level methods such as post-
21
22 Hartree-Fock (PHF) techniques¹⁶ or many-body perturbation theory at the GW-BSE level.¹⁷
23
24 Available experimental data for TADF molecules indicate that the singlet-triplet splitting ΔE_{ST}
25
26 can be as small as 0.1 eV,¹⁰ which requires that the theoretical methodologies be able to provide
27
28 quantitative predictions.
29
30
31
32
33

34
35
36 On the other hand, time-dependent density functional theory (TDDFT)^{18, 19} is a well-established
37
38 tool to study the excited states of relatively large molecular systems and affords a reasonable
39
40 compromise between accuracy and computational cost.²⁰ However, when dealing with donor-
41
42 acceptor molecules with charge-transfer (CT) characteristics, TDDFT calculations based on
43
44 standard functionals can severely underestimate the excitation energies.²¹ In general, these
45
46 systematic errors can be attributed to the introduction of inappropriate exchange-correlation (XC)
47
48 approximations and can be further traced back to large electron self-interaction or delocalization
49
50 error (DE)^{22, 23} and lack of derivative discontinuity (DD),²⁴ as well as to an incorrect behavior of
51
52 the electron-electron potential at asymptotically large distances.^{25, 26} The introduction of a
53
54
55
56
57
58
59
60

1
2
3 suitable, fixed amount of exact-exchange (eX) has been shown to provide an improved
4 description of the excited-state properties.¹⁰ The vertical transition energies of the first singlet
5 states in TADF molecules and the (closely related) electronic-coupling (or transfer-integral)
6 parameters in organic molecular crystals have been shown to be very sensitive to the amount of
7 eX.^{10, 27, 28} Thus, an appropriate balance between the eX from Hartree-Fock and electron
8 correlation from DFT is crucial to achieve reliable estimates of π -conjugated electronic
9 structures.²⁹ As such, the issue becomes how to determine such a balance and how much eX
10 should be included for a specific system.
11
12
13
14
15
16
17
18
19
20
21
22
23

24 Recently, the development of range-separated exchange (RS)³⁰ density functionals has allowed
25 the mitigation of the CT issue with TDDFT.^{29, 31, 32} The general expression of RS functionals
26 provides a theoretical framework based on which one can adjust the parameters in Equation (1)
27 to tune the percentages of eX. In such functionals, a three-parameter expression of the
28 interelectronic distance r_{12} is used for the separation of the exchange term into a short-range
29 domain and a long-range domain:²⁵
30
31
32
33
34
35
36
37
38
39
40
41

$$\frac{1}{r_{12}} = \frac{1 - [\alpha + \beta \operatorname{erf}(\omega r_{12})]}{r_{12}} + \frac{\alpha + \beta \operatorname{erf}(\omega r_{12})}{r_{12}} \quad (1)$$

42
43
44
45
46
47
48
49 Thus, the exchange term is split into a long-range exact exchange (eX) component coming from
50 Hartree-Fock and a short-range DFT component derived from local-density or generalized-
51 gradient approximations (LDA or GGA). The parameter α quantifies the fraction of eX in the
52 short-range limit, while $\alpha + \beta$ gives the fraction of eX in the long-range limit. The range-
53
54
55
56
57
58
59
60

1
2
3 separation parameter ω represents the inverse of the distance at which the exchange term
4 switches from DFT-like to HF-like. The ω values in RS functionals have been shown to be
5 strongly system-dependent, in particular in the case of π -conjugated systems.³³⁻³⁵ Baer, Kronik,
6 and their collaborators have considered a nonempirical criterion to determine the optimal ω in
7 RS functionals.³⁶ The concept of “optimal tuning” corresponds to adjusting ω to fulfill a
8 fundamental property that the exact functional must obey in exact Kohn-Sham (KS) or
9 generalized KS (GKS) theory: for an N -electron system, the negative of the HOMO energy
10 $-\varepsilon_H(N)$ must equal the molecular vertical ionization potential (IP).³⁷ For a given system, the
11 optimal ω value can hence be obtained without empirical fitting by minimizing Expression 2a:
12
13
14
15
16
17
18
19
20
21
22
23
24
25
26

$$J = |\varepsilon_H(N) + IP(N)| \quad (2a)$$

27
28
29
30
31 In donor-acceptor systems, it is useful to focus not only on the ionization potential (essentially
32 related to the donor component) but also on the electron affinity (essentially related to the
33 acceptor component). The vertical electron affinity (i.e., in the absence of geometry relaxation)
34 of the N -electron system can be considered as the ionization potential of the $N + 1$ -electron
35 system. In this context, the tuning of ω value can be done on the basis of Expression 2b:³⁸
36
37
38
39
40
41
42
43
44
45

$$J^2 = \sum_{i=0}^1 [\varepsilon_H(N + i) + IP(N + i)]^2 \quad (2b)$$

46
47
48
49
50
51 which is used throughout this work. The optimally-tuned range-separated DFT method has been
52 successfully used in cases generally considered challenging for (TD)DFT.^{22, 23} In addition, the
53 Tamm-Dancoff Approximation (TDA)³⁹⁻⁴¹ scheme of TD-DFT has been recently shown to
54
55
56
57
58
59
60

1
2
3 provide reliable absorption and emission spectra⁴² and especially better estimates of the lowest
4
5 singlet-triplet energy gaps,⁴³ which is relevant for TADF systems.
6
7
8
9

10 In this work, our goal is to demonstrate the predictive ability of TD(A)-DFT calculations using
11 nonempirically tuned RS functionals for the vertical (absorption) excitation energies of the first
12 singlet excited states $E_{VA}(S_1)$ and the corresponding singlet-triplet gaps ΔE_{ST} . The calculations
13 are carried out for a series of 17 molecules whose chemical structures are shown in Scheme 1.
14
15 This series consists of : (i) 4 molecules with relatively large singlet-triplet gaps (ΔE_{ST}
16 =0.55~0.80 eV), usually used as hole/electron transporting layers; (ii) 8 molecules with moderate
17 gaps (ΔE_{ST} =0.15~0.50 eV); and (iii) 5 molecules with very small gaps (ΔE_{ST} =0.00~0.10 eV),
18 which can be considered as representative TADF emitters. All these molecules are typical donor-
19 acceptor CT molecules, mainly based on fragments such as carbazolyl (Cz), triphenylamine
20 (NPh₃), 1,3,5-triazine (TRZ), or dicyanobenzene (DCB). The molecular structures are such that
21 adjacent donor and acceptor units, due to steric hindrance, can be strongly out of plane.
22
23 Therefore, such structures are prone to lead to spatial separations of HOMOs and LUMOs, which
24 can lead to small ΔE_{ST} values. We note that, in addition, calculations using conventional
25 functionals are also performed for the sake of comparison.
26
27
28
29
30
31
32
33
34
35
36
37
38
39
40
41
42
43
44
45
46
47
48
49
50
51
52
53
54
55
56
57
58
59
60

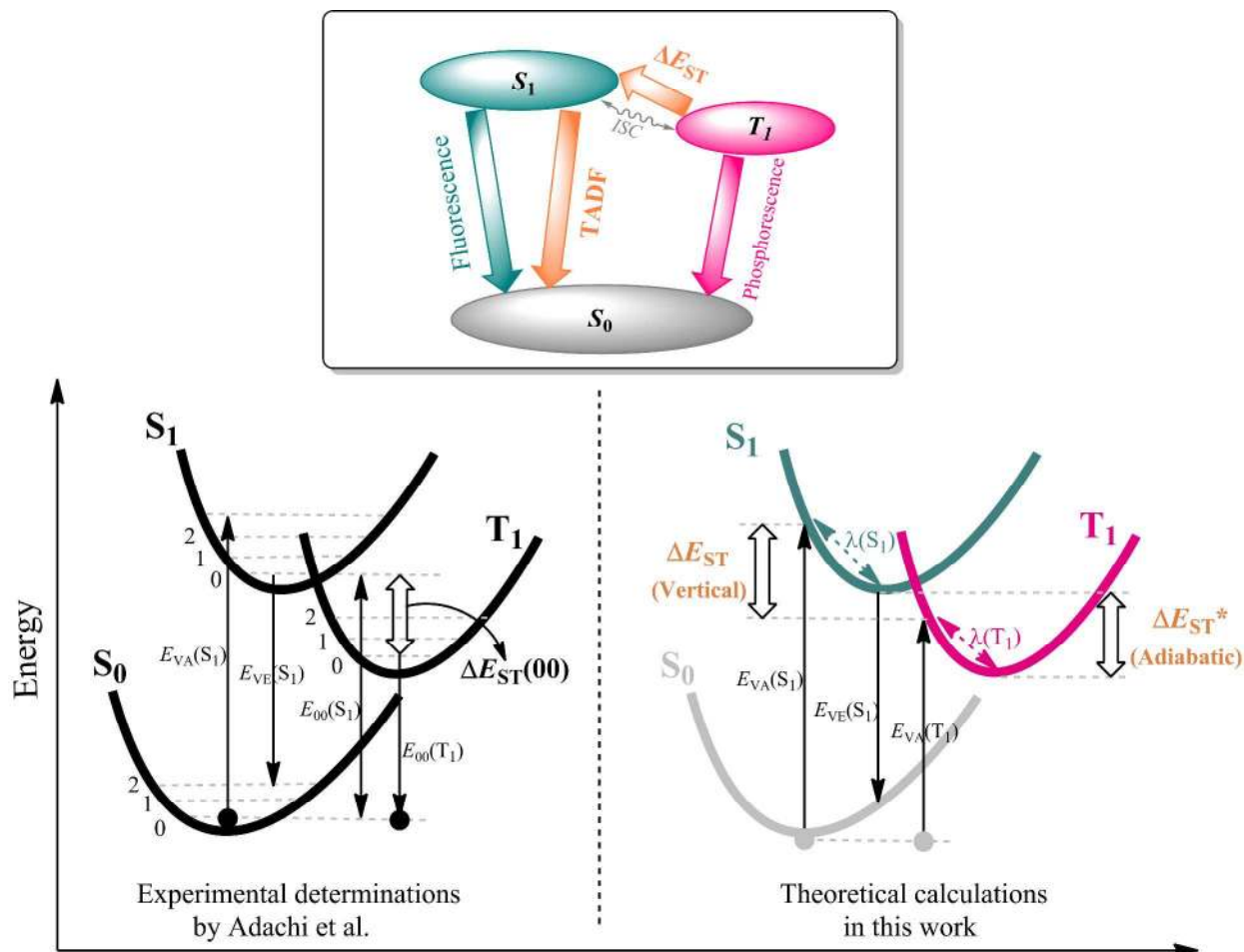
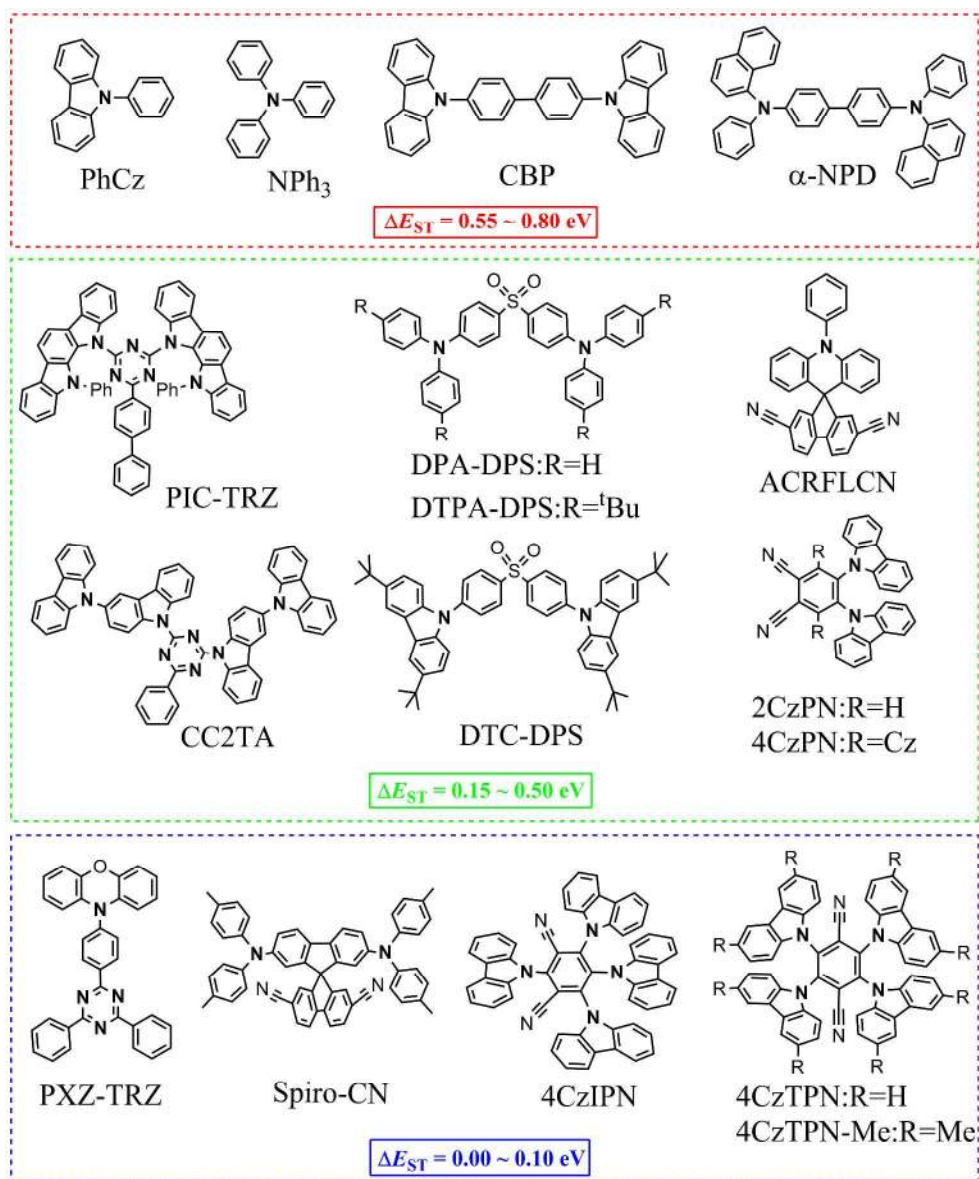


Figure 1. Schematic representation (top) and potential energy surfaces (bottom) of the photophysical processes in thermally activated delayed fluorescence (TADF) compounds. S_0 : singlet ground state; S_1 : lowest singlet excited state; T_1 : lowest triplet excited state; ISC: intersystem crossing. VA: vertical absorption; VE: vertical emission; $\lambda(S_1)$ and $\lambda(T_1)$: relaxation energies of S_1 and T_1 .



Scheme 1. Chemical structures of the molecules investigated in this work. The experimental singlet-triplet gaps are taken from the work of Adachi and co-workers.¹⁰

2. Computational Details

Ground-state geometries for all the molecules collected in Scheme 1 (taken from the work by Adachi et al.¹⁰) are optimized at the B3LYP/6-31G(d) level. The optimal ω values were determined based on the LC- ω PBE functional with the 6-31+G(d) basis set and are listed in Table 1. Hereafter, we refer to the optimally tuned functional as LC- ω PBE*. The optimal ω values appear not to be sensitive to extension of the basis set from 6-31G(d) to 6-31+G(d) (Table S1 in Supporting Information, SI). For the optimization of the range-separation parameter ω , all the single-point calculations were carried out for the N and $N \pm 1$ systems using the default SCF convergence criteria in the Gaussian 09 code.⁴⁴ An original “Golden proportion” approach (see SI for details) was developed to obtain the optimal ω value that minimizes J^2 in Equation 2b (note that the search for optimal ω values was limited to the range 0.05 - 0.5 Bohr⁻¹).

The vertical excitation (absorption) energies of the lowest singlet- ($E_{VA}(S_1)$) and triplet- ($E_{VA}(T_1)$) excited states are calculated using linear-response TD-DFT or the TDA approach with the 6-31+G(d) basis set. The vertical singlet-triplet splitting is accordingly obtained as $\Delta E_{ST} = E_{VA}(S_1) - E_{VA}(T_1)$. In order to take into account the effects of the dielectric medium, we have tested the polarizable continuum model (PCM)⁴⁵ using the default linear-response method as well as the recently developed state-specific (SS) approach⁴⁶ in the calculations of excitation energies, as shown in Table S2. We find that, while requiring additional computational efforts, the SS method does not produce any significant improvement on the prediction of the $E_{VA}(S_1)$ values compared to the linear-response method. Therefore, the PCM approach using the default linear-response method is employed in the calculations of excitation energies discussed in this work.”

1
2
3
4
5
6 The basis-size effects were examined by extending the basis sets from 6-31G(d) to 6-31+G(d),
7
8 6-311G(d), 6-311+G(d), and 6-311++G(d,p) (see Table S2). The 6-31+G(d) basis shows a good
9
10 balance between accuracy of the results and reasonable computational cost. It should be noted
11
12 that most of the experimental ΔE_{ST} values are deduced from delayed fluorescence or
13
14 phosphorescence spectra taken in solution (usually in toluene); therefore, they are related to
15
16 $E_{00}(S_1)$ and $E_{00}(T_1)$, which involve excited-state geometry relaxations, as shown in Figure 1. We
17
18 thus carried out calculations of the adiabatic ΔE_{ST}^* values, which are defined as the energy
19
20 differences between the minima potential energies of the S_1 and T_1 states. The geometries of the
21
22 S_1 states are optimized using the implemented TD-DFT gradients at the PCM (toluene)-CAM-
23
24 B3LYP/6-31G(d) level; the geometries of the T_1 states are assessed by spin-relaxed open-shell
25
26 optimizations at the UCAM-B3LYP/6-31G(d) level (also considering toluene as the dielectric
27
28 medium). The reason why we employed the CAM-B3LYP functional is related to the fact that
29
30 the TADF molecules considered here are mostly donor-acceptor charge-transfer molecules and
31
32 B3LYP would significantly overestimate electron delocalization in the excited states. The results
33
34 in Table S3 show that, in comparison to full TDDFT, the corresponding TDA approach with
35
36 tuned LC- ω PBE* functionals gives a slightly improved description of the singlet-triplet splittings
37
38 ΔE_{ST} with respect to the experimental data, due to the better description of the triplet excitation
39
40 energies within the TDA approach.⁴³ Considering its lower computational cost and the
41
42 possibility of avoiding the triplet instability issue,⁴² the TDA scheme is employed here for all the
43
44 calculations of excitation energies. Therefore, except explicitly stated otherwise, all the ΔE_{ST}
45
46 calculations were carried out at the PCM (toluene)-TDA-DFT/6-31+G(d) level.
47
48
49
50
51
52
53
54
55
56
57
58
59
60

1
2
3 To examine to what extent the TDA results based on ground-state geometries optimized with
4 different functionals change, we have calculated the singlet and triplet excitation energies using
5 the optimally-tuned LC- ω PBE* functional based on the ground-state geometries optimized with
6 LC- ω PBE*, B3LYP, and CAM-B3LYP, and compared the results to the corresponding
7 experimental data, see Table S4. We find that the calculated excitation energies remain close
8 regardless of the functionals used for the ground-state geometry optimizations. This finding is
9 consistent with recent studies by Tamblyn et al.⁴⁶ and Adachi et al.¹⁰ To test the performance of
10 various density functionals and the influence of eX percentages (eX%), we performed
11 calculations with seven functionals at different levels of Perdew's Jacob's ladder⁴⁸: a pure
12 generalized gradient approximation (GGA) functional, PBE⁴⁹ (0%); a hybrid-GGA functional,
13 B3LYP^{50, 51} (20%); two meta-GGA functionals, M062X⁵² (56%) and M06HF⁵³ (100%); and
14 three range-separated functionals, CAM-B3LYP²⁵ ($\alpha=0.19$, $\alpha+\beta=0.65$, short range ~ long range:
15 19% ~ 65%), LC- ω PBE⁵⁴ ($\alpha=0.0$, $\alpha+\beta=1.0$, 0% ~ 100%), and ω B97XD^{31, 55} ($\alpha=0.22$, $\alpha+\beta=1.0$,
16 22% ~ 100%). Figure 2 displays the percentage of eX included as a function of interelectronic
17 distance (r_{12}) for various functionals. Recent results⁴³ using double-hybrid density functionals
18 which lie on the top level of the DFT "ladder" are also included in the discussion for the sake of
19 comparison.
20
21
22
23
24
25
26
27
28
29
30
31
32
33
34
35
36
37
38
39
40
41
42
43
44
45
46
47
48
49
50
51
52
53
54
55
56
57
58
59
60

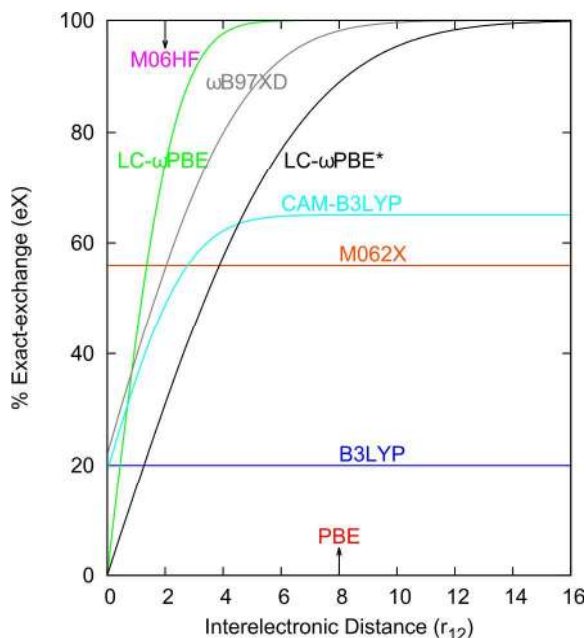


Figure 2. Percentage of exact-exchange (eX) included as a function of interelectronic distance (r_{12} , Bohr) for various functionals. The LC- ω PBE* curve is taken from the calculation on PIC-TRZ with an optimal ω value of 0.141 Bohr⁻¹.

3. Results and Discussion

Table 1 lists the optimal ω values, the calculated vertical absorption energies $E_{VA}(S_1)$, the vertical ΔE_{ST} and adiabatic ΔE_{ST}^* values, and their mean absolute deviation (MAD) values using the LC- ω PBE* and non-tuned LC- ω PBE results vs. the experimental data. For comparison, the detailed results using the other density functionals are reported in Table S6. The optimal ω values are in the range from 0.141 (PIC-TRZ) to 0.204 (PhCz) Bohr⁻¹; they are thus significantly smaller than the default ω value for LC- ω PBE (0.400 Bohr⁻¹), indicating that the tuned functional switches from DFT to eX at larger interelectronic distances; in other words, the short-range DFT component is more slowly replaced by eX. These results confirm the necessity of “tuning” ω since smaller ω values are required for a proper description of the TADF molecules in this work. The default parameters for other popular RS functionals (0.330 Bohr⁻¹ for CAM-

1
2
3 B3LYP and 0.200 Bohr⁻¹ for ω B97XD) are still (somewhat) larger than is optimal. Our results in
4
5 Table 1 show that in comparison to the non-tuned LC- ω PBE functional (with MADs of 1.03 eV
6
7 for $E_{\text{VA}}(\text{S}_1)$, 0.73 eV for ΔE_{ST} , and 0.70 eV for ΔE_{ST}^*), the corresponding optimally tuned
8
9 version can significantly reduce the errors by up to one order of magnitude, with MADs of 0.15
10
11 eV for $E_{\text{VA}}(\text{S}_1)$, 0.07 eV for ΔE_{ST} , and 0.09 eV for ΔE_{ST}^* .
12
13
14
15
16
17
18
19
20
21
22
23
24
25
26
27
28
29
30
31
32
33
34
35
36
37
38
39
40
41
42
43
44
45
46
47
48
49
50
51
52
53
54
55
56
57
58
59
60

Table 1. Calculated $E_{VA}(S_1)$ and $E_{VA}(T_1)$ values and vertical singlet-triplet gaps ΔE_{ST} and adiabatic singlet-triplet gaps ΔE_{ST}^* in comparison to experimental data.^a

		PCM(toluene)-TDA-DFT/6-31+G(d) level						Exp. values ^b		
		LC- ω PBE ($\omega = 0.400$)			LC- ω PBE*			$E_{VA}(S_1)$	$\Delta E_{ST}(00)$	
Compound	ω^* ^a	$E_{VA}(S_1)$	ΔE_{ST}	ΔE_{ST}^*	$E_{VA}(S_1)$	ΔE_{ST}	ΔE_{ST}^*			$E_{VA}(S_1)$
L	PhCz	0.204	4.66	1.20	1.19	4.17	0.73	0.75	3.66	0.55
	NPh ₃	0.198	4.71	1.21	1.22	3.98	0.61	0.74	3.74	0.57
	CBP	0.173	4.62	1.26	1.33	3.94	0.66	0.88	3.80	0.71
	α -NPD	0.170	4.17	1.31	1.51	3.29	0.57	0.76	3.31	0.73
	PIC-TRZ	0.141	4.28	1.09	0.91	3.17	0.22	0.11	3.35	0.18
	DPA-DPS	0.166	4.33	1.04	0.98	3.60	0.60	0.49	3.53	0.52
	DTPA-DPS	0.152	4.28	1.02	1.11	3.48	0.56	0.46	3.47	0.46
M	ACRFLCN	0.174	4.52	1.50	1.35	3.03	0.07	0.02	3.05	0.24
	CC2TA	0.159	4.54	1.14	0.86	3.66	0.35	0.13	3.64	0.20
	DTC-DPS	0.160	4.51	1.09	1.27	3.60	0.39	0.27	3.62	0.36
	2CzPN	0.176	4.20	1.06	1.24	3.22	0.41	0.24	3.19	0.31
	4CzPN	0.146	3.96	0.92	1.02	2.55	0.13	0.00	2.82	0.15
S	PXZ-TRZ	0.183	4.10	0.94	0.60	2.94	0.07	0.01	2.73	0.06
	Spiro-CN	0.168	3.97	1.08	0.89	2.73	0.07	0.01	2.69	0.06
	4CzIPN	0.142	3.84	0.75	0.73	2.52	0.12	0.01	2.85	0.10
	4CzTPN	0.147	3.63	0.59	0.70	2.32	0.14	0.06	2.61	0.09
	4CzTPN-Me	0.143	3.69	0.63	0.43	2.28	0.12	0.09	2.49	0.09
MAD ^c			1.03	0.73	0.70	0.15	0.07	0.09		

^a Optimal range-separation parameter ω^* (Bohr⁻¹) used in the LC- ω PBE* calculations. ^b Experimental data are taken from ref¹⁰. ^c The MAD values are calculated with respect to the corresponding experimental values. The labels L, M, and S refer to molecules with relatively large, medium, and small singlet-triplet gaps, respectively.

Table 2. Statistical analysis including mean absolute deviations (MAD, eV), relative errors (RE), and linear correlation coefficients (R^2) obtained from the comparison between theoretical and experimental data.^a

Functional	$E_{VA}(S_1)$			ΔE_{ST}			ΔE_{ST}^*		
	MAD	RE(%)	R^2	MAD	RE(%)	R^2	MAD	RE(%)	R^2
PBE	0.95	31	0.67	0.17	52	0.50	0.28	105	0.22
B3LYP	0.39	13	0.87	0.10	36	0.73	0.16	73	0.74
M062X	0.43	14	0.96	0.09	48	0.85	0.10	57	0.89
M06HF	1.04	34	0.72	0.25	197	0.27	0.34	228	0.38
CAM-B3LYP	0.49	16	0.97	0.26	144	0.77	0.19	71	0.94
ω B97XD	0.61	19	0.94	0.30	187	0.69	0.24	101	0.91
LC- ω PBE	1.03	33	0.80	0.73	473	0.31	0.70	409	0.57
LC- ω PBE*	0.15	5	0.91	0.07	27	0.85	0.09	41	0.93

$$^a \text{MAD} = \frac{1}{n} \sum_i^n |\Delta E_{cal} - \Delta E_{exp}| \text{ and } \text{RE} = \frac{1}{n} \sum_i^n \left| \frac{\Delta E_{cal} - \Delta E_{exp}}{\Delta E_{exp}} \right|.$$

In Table 2, the results of statistical analyses including the mean absolute deviations (MAD), relative errors (RE), and linear correlation coefficients (R^2) between the theoretical and experimental data, are collected for the other functionals considered in this work. The histograms in Figures S1-S3 are also plotted for better visualization of the errors distributions. For the lowest singlet excitation energies, except for the pure GGA PBE and hybrid B3LYP, all these functionals consistently overestimate the $E_{VA}(S_1)$ values. PBE with 0% eX and the meta-GGA M06HF with 100% eX produce very large MADs of 0.95 and 1.04 eV, respectively, and relatively large percentages of RE (31% and 34%). The hybrid B3LYP and M062X functionals, which include a fixed amount of eX, reduce the MADs and REs by about half (0.39 and 0.43 eV; 13% and 14%), which confirms the pivotal effect of considering an “optimal” percentage of exact exchange in the electronic-structure methodology.^{10, 43} The untuned RS functionals such as CAM-B3LYP and ω B97XD produce slightly greater errors compared to the hybrid B3LYP and

1
2
3 M062X functionals. Except for PBE and M06HF, all the functionals provide a reasonably high
4
5 linear correlation coefficient R^2 (0.80~0.97) between the calculated and experimental data.
6
7

8
9
10 For the singlet-triplet gaps, we first analyze the performance of functionals in the prediction of
11
12 the vertical ΔE_{ST} values and then turn to the adiabatic ΔE_{ST}^* values which include relaxation
13
14 effects. It should be noted that, in comparison to the pure GGA and hybrid GGA functionals, all
15
16 the RS functionals produce rather large MADs (0.26~0.73 eV) and REs (144%~473%). The
17
18 B3LYP and M062X functionals seem to produce small deviations (0.09~0.10 eV). The good
19
20 performance using M062X functional is also observed by Jacquemin and collaborators.⁵⁶
21
22 However, when considering the relatively large MADs of the $E_{VA}(S_1)$ values using B3LYP (0.39
23
24 eV) and M062X (0.43 eV), their small MADs are mainly attributed to an error cancellation
25
26 resulting from the simultaneous under-/overestimation of singlet and triplet excitation energies.
27
28 For the description of the ΔE_{ST}^* values, all the functionals show similar performance as for the
29
30 vertical ΔE_{ST} values. It is worth noting that negative ΔE_{ST}^* values are observed using PBE and
31
32 B3LYP (as shown in Table S6), which results in significantly larger MADs and REs in
33
34 comparison to the results for the vertical ΔE_{ST} . Overall, the functionals adopting conventional
35
36 XC approximations give in consistent results in going from one system to another, which calls
37
38 into question their reliability in the prediction of the properties of new TADF molecules.
39
40 Importantly, the optimally-tuned LC- ω PBE* functional delivers both the smallest MADs
41
42 (0.15eV for the $E_{VA}(S_1)$, 0.07 eV for the vertical ΔE_{ST} , and 0.09 eV for the adiabatic ΔE_{ST}^*) and
43
44 lowest REs (5%, 27%, and 41%) and also comes with high R^2 values (0.91, 0.85, and 0.93). In
45
46 addition, the plots of error distributions present a Gaussian shape with a peak position around
47
48 zero (see Figures S1-S3), which demonstrates the reliability of an optimally tuned RS functional.
49
50
51
52
53
54
55
56
57
58
59
60

1
2
3 A recent study by Moral et al.⁴³ using “state-of-the-art” double-hybrid functionals (B2-PLYP
4 and B2GP-PLYP) shows that the MADs for the $E_{VA}(S_1)$ values collected for six selected
5 molecules (PhCz, NPh₃, ACRFLCN, CBP, 2CzPN and PXZ-TRZ) are 0.34 and 0.28 eV,
6 respectively. Thus, it appears that the errors are not significantly reduced compared to those of
7 the tuned functional. The errors between the calculated $E_{VA}(S_1)$ values using LC- ω PBE* and
8 experimental values and their distributions are presented in Table 1 and Figure S1. It can be seen
9 that for 8 of the 17 molecules studied in this work, the differences are < 0.1 eV and, for 8 other
10 ones, they are in the range of roughly 0.1 ~ 0.3 eV. All these errors distribute as a Gaussian with
11 the peak around zero. Interestingly, there is one molecule, PhCz, for which a larger error of 0.51
12 eV is found: calculated $E_{VA}(S_1)$ value of 4.17 eV vs. an experimental estimate of 3.66 eV. Thus,
13 we also performed high-level calculations of the vertical singlet excitation energy in PhCz with
14 second-order approximate coupled-cluster (CC2) theory and considered the results using double-
15 hybrid functionals taken from the work by Moral et al.⁴³ As shown in Table S5, the results from
16 the high-level methods are close to those from tuned LC- ω PBE* (CC2: 3.98 eV, B2-PLYP: 3.98
17 eV, and B2GP-PLYP: 4.15 eV). It is clearly of interest to employ such well-established, reliable
18 high-level methods to benchmark the excitation energies for TADF molecules; however, their
19 main challenge comes from their very high computational costs when the molecular size
20 becomes large. That a comparable level of accuracy is obtained when using the optimal-tuning
21 approach again confirms its clear benefit given its relatively low computational cost. By taking
22 into account the overall performance of the representative functionals selected from the Jacob’s
23 ladder of DFT, the optimally tuned RS functional significantly outperforms all the other types of
24 functionals and achieves excellent accuracy at reasonable computational cost.
25
26
27
28
29
30
31
32
33
34
35
36
37
38
39
40
41
42
43
44
45
46
47
48
49
50
51
52
53
54
55
56
57
58
59
60

1
2
3 To analyze the extent of excited-state geometry relaxations, we present the relaxation energies
4 $\lambda(S_1)$ and $\lambda(T_1)$ for the S_1 and T_1 states, respectively, in Figure 1 and Table S7. The relaxation
5 effects are seen to be system-dependent with the mean values for $\lambda(S_1)$ and $\lambda(T_1)$ collected for all
6 17 molecules being 0.17 and 0.13 eV, respectively. It is worthwhile to recall that extended, linear
7 π -conjugated molecules have similar relaxation energies in the S_1 state but usually display
8 substantially larger relaxations in the T_1 state (due to a stronger localization of the T_1
9 wavefunction), which leads to ΔE_{ST} values in the range 0.7-1.0 eV.^{57, 58} Interestingly, the
10 molecules with a large ΔE_{ST} are those where small $\lambda(S_1)$ values are accompanied by larger $\lambda(T_1)$
11 values. Conversely, the molecules with small ΔE_{ST} possess relatively larger $\lambda(S_1)$ values,
12 indicating more pronounced geometry relaxation in the S_1 state. We then plot the hole/electron
13 distributions of S_1 and T_1 for the two representative molecules: CBP ($\lambda(S_1)$ =0.18 eV and
14 $\lambda(T_1)$ =0.40 eV) and CC2TA ($\lambda(S_1)$ =0.29 eV and $\lambda(T_1)$ =0.07 eV) in Scheme S1 of the SI. A
15 more localized character is found in the T_1 state of CBP and the S_1 state of CC2TA, respectively.
16 As shown in Table S8, all S_1 transitions are characteristic of typical CT excitations. For the T_1
17 states, our results show a significant local-excitation (LE) character; this is in agreement with the
18 experimental assignments except for PIC-TRZ, 4CzPN, and 4CzIPN¹⁰ (it should be borne in
19 mind, however, that it may be difficult to make accurate assignments of the T_1 states when the
20 experimental bands show a not well-defined shape with low resolution).
21
22
23
24
25
26
27
28
29
30
31
32
33
34
35
36
37
38
39
40
41
42
43
44
45
46
47

48 Next, from the perspective of the eX percentages included in the investigated functionals, we try
49 to analyze the reason why different functionals produce different sizes of error. As seen in Figure
50 2, at r_{12} values between 2.5 and 3 Bohr (roughly 1.322 ~ 1.587 Å), which is the range of carbon-
51 carbon single and double bonds, the LC- ω PBE* functional affords roughly 45% eX while the
52
53
54
55
56
57
58
59
60

1
2
3 non-tuned LC- ω PBE with a default ω of 0.4 gives almost 90% eX, which points to LC- ω PBE as
4 being HF-like; at similar distances, the CAM-B3LYP and ω B97XD functionals contain roughly
5
6 60% and 70% eX, respectively. These percentages of eX included in the functionals are found to
7
8 be consistent with the size of the errors; in other words, the higher the eX%, the greater the errors,
9
10 which confirms the findings of Mortal et al.⁴³ It can be concluded that the overall overestimation
11
12 of $E_{\text{VA}}(\text{S}_1)$ and ΔE_{ST} with commonly used RS functionals is related to their more HF-like
13
14 character. In this regard, the slightly better performance of B3LYP and M062X can also be
15
16 attributed to a suitable amount of eX.
17
18
19
20
21
22
23

24 It has been shown that the problems posed by (TD-)DFT are closely related to violations of basic
25 conditions of constraints.⁵⁹ In exact Kohn-Sham theory, the energy of an atom or molecule as a
26 function of electron number $E(N)$ should afford straight-line segments between integers.
27
28 However, commonly-used functionals with inappropriate XC kernels tend to over-/under-
29
30 estimate the delocalization effect of holes/electrons and produce a so-called delocalization error
31
32 (DE). This error can be quantitatively characterized by the curvature of $E(N)$ as shown in Figure
33
34 3. Here, the behavior of $E(N)$ is examined for PhCz as a representative example. The results are
35
36 as expected: the pure GGA PBE and global hybrid B3LYP functionals produce large positive
37
38 curvatures of $E(N)$, indicating that these functionals provide too delocalized wavefunctions.
39
40 Magnitude-wise, the M062X and CAM-B3LYP functionals produce a less pronounced DE
41
42 compared to conventional PBE and B3LYP. Interestingly, for the M06HF and LC- ω PBE
43
44 functionals, the DEs are also improved but afford obvious negative curvatures, indicating a
45
46 somewhat too localized, HF-like character. Overall, the optimally tuned LC- ω PBE* reduces the
47
48
49
50
51
52
53
54
55
56
57
58
59
60

DE to a minimum. The results confirm that reducing the delocalization error and thus the many-electron self-interaction error, is an additional indicator to select the optimal functionals.^{22, 60}

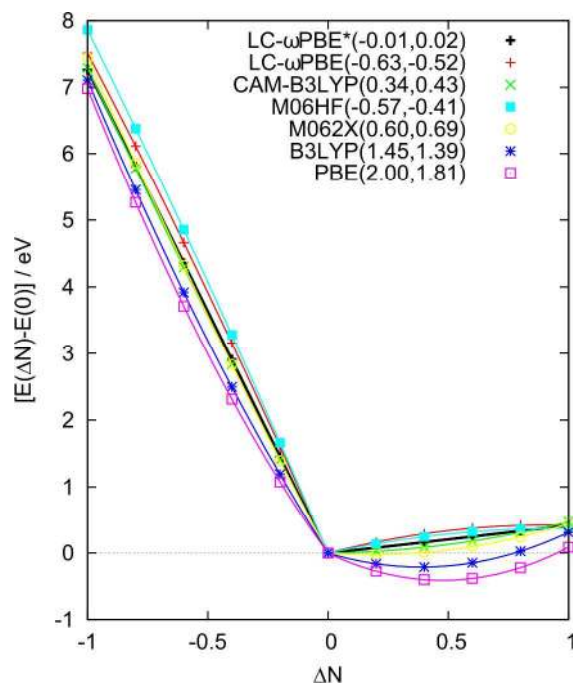


Figure 3. Energy of the PhCz molecule as a function of the fractional electron number, ΔN , relative to the neutral system ($\Delta N = 0$). The numerical values in the plot correspond to the coefficients of $(\Delta N)^2$ of quadratic fits to $E(N)$ in the electron-deficient and electron-rich regime, respectively ($\Delta N < 0$, $\Delta N > 0$). The calculations are performed using the developmental version of the NWChem package.⁶¹

4. Conclusions and Outlook

We have demonstrated the efficiency of a nonempirically tuned range-separated exchange functional in reproducing the experimental lowest singlet excitation energies and the corresponding singlet-triplet gaps (derived from 0-0 transitions) for a series of 17 TADF emitters.

With respect to the experimental data, the optimally-tuned RS functional lead to very good

1
2
3 theoretical estimates with MADs of 0.15 eV for the $E_{VA}(S_1)$ values, 0.07 eV for the vertical ΔE_{ST}
4 values, and 0.09 eV for the adiabatic ΔE_{ST}^* values. In addition, high correlation coefficient
5 values R^2 (0.91, 0.85, and 0.93, respectively) are obtained. The plots of error distributions using
6 the tuned functional present standard Gaussian shapes with the peak positions always around
7 zero. The performance of the optimally-tuned functional is clearly superior to the non-tuned
8 version, confirming the positive impact of the tuning. Commonly used RS functionals such as
9 ω B97XD and CAM-B3LYP, when considering default ω values, greatly overestimate the
10 vertical excitation energies (MADs of $> \sim 0.5$ eV) and produce relatively large MADs and
11 relative errors for singlet-triplet gaps, which is mainly due to their high eX%. For non-RS
12 functionals, both the pure GGA PBE functional and M06HF, which contain 0% and 100% eX,
13 respectively, produce very large deviations (MADs $> \sim 1.0$ eV for the vertical excitation energies
14 and MADs $> \sim 0.20$ eV for the singlet-triplet gaps), as well as large relative error values and low
15 correlation coefficients. Compared to PBE and M06HF, hybrid functionals such as B3LYP and
16 M062X overall give improved predictions, especially for the singlet-triplet gaps, which can be
17 attributed to a suitable amount of eX; however, the good performance in predicting singlet-triplet
18 gaps using M062X and B3LYP can be attributed to a simultaneous over-/underestimation of the
19 lowest singlet and triplet excitation energies.
20
21
22
23
24
25
26
27
28
29
30
31
32
33
34
35
36
37
38
39
40
41
42
43
44

45 To summarize, as it combines reliable estimates of the relevant energies with reasonable
46 computational costs, an optimally tuned RS functional is seen as a useful tool in the design and
47 prediction of novel TADF chromophores. In addition, because of its reliability in predicting both
48 singlet and triplet excitation energies, an optimally-tuned method can be explored for the
49
50
51
52
53
54
55
56
57
58
59
60

1
2
3 description of singlet fission in organic semiconductors, which also requires quantitative
4
5 assessments of singlet and triplet excited states.
6
7
8
9

10 11 12 13 **Acknowledgments**

14
15
16
17 This work has been supported by King Abdullah University of Science and Technology
18 (KAUST). We acknowledge the KAUST IT Research Computing Team for providing
19
20 computational and storage resources and thank Dr. Bradley Rose and Dr. Yuan Li for stimulating
21
22 discussions.
23
24
25
26
27
28
29
30
31

32 **References:**

- 33
34 (1) Bent, H. A. *Chem. Rev.*, **1968**, *68*, 587-648.
35 (2) Brédas, J.-L. *Science*, **1994**, *263*, 487-488.
36 (3) Tseng, H.-R.; Ying, L.; Hsu, B. B. Y.; Perez, L. A.; Takacs, C. J.; Bazan, G. C.; Heeger,
37 A. J. *Nano Letters*, **2012**, *12*, 6353-6357.
38 (4) Yu, G.; Gao, J.; Hummelen, J. C.; Wudl, F.; Heeger, A. J. *Science*, **1995**, *270*, 1789-
39 1791.
40 (5) Lima, I. T.; Risko, C.; Aziz, S. G.; da Silva Filho, D. A.; Bredas, J.-L. *J. Mater. Chem. C*,
41 **2014**, *2*, 8873-8879.
42 (6) Uoyama, H.; Goushi, K.; Shizu, K.; Nomura, H.; Adachi, C. *Nature*, **2012**, *492*, 234-238.
43 (7) Hirata, S.; Sakai, Y.; Masui, K.; Tanaka, H.; Lee, S. Y.; Nomura, H.; Nakamura, N.;
44 Yasumatsu, M.; Nakanotani, H.; Zhang, Q.; Shizu, K.; Miyazaki, H.; Adachi, C. *Nat. Mater.*,
45 **2015**, *14*, 330-336.
46 (8) Nakanotani, H.; Higuchi, T.; Furukawa, T.; Masui, K.; Morimoto, K.; Numata, M.;
47 Tanaka, H.; Sagara, Y.; Yasuda, T.; Adachi, C. *Nat. Commun.*, **2014**, *5*.
48 (9) Tanaka, H.; Shizu, K.; Nakanotani, H.; Adachi, C. *Chem. Mater.*, **2013**, *25*, 3766-3771.
49 (10) Huang, S.; Zhang, Q.; Shiota, Y.; Nakagawa, T.; Kuwabara, K.; Yoshizawa, K.; Adachi,
50 C. J. *Chem. Theory Comput.*, **2013**, *9*, 3872-3877.
51 (11) Friend, R. H.; Gymer, R. W.; Holmes, A. B.; Burroughes, J. H.; Marks, R. N.; Taliani,
52 C.; Bradley, D. D. C.; Santos, D. A. D.; Brédas, J. L.; Logdlund, M.; Salaneck, W. R. *Nature*,
53 **1999**, *397*, 121-128.
54
55
56
57
58
59
60

- 1
2
3
4
5
6
7
8
9
10
11
12
13
14
15
16
17
18
19
20
21
22
23
24
25
26
27
28
29
30
31
32
33
34
35
36
37
38
39
40
41
42
43
44
45
46
47
48
49
50
51
52
53
54
55
56
57
58
59
60
- (12) Zhang, Q.; Li, B.; Huang, S.; Nomura, H.; Tanaka, H.; Adachi, C. *Nat. Photon.*, **2014**, *8*, 326-332.
- (13) Chen, X.-K.; Zhang, S.-F.; Fan, J.-X.; Ren, A.-M. *J. Phys. Chem. C*, **2015**, *119*, 9728-9733.
- (14) Endo, A.; Ogasawara, M.; Takahashi, A.; Yokoyama, D.; Kato, Y.; Adachi, C. *Adv. Mater.*, **2009**, *21*, 4802-4806.
- (15) Dreuw, A.; Head-Gordon, M. *Chem. Rev.*, **2005**, *105*, 4009-4037.
- (16) Kánnár, D.; Szalay, P. G. *J. Chem. Theory Comput.*, **2014**, *10*, 3757-3765.
- (17) Samsonidze, G.; Jain, M.; Deslippe, J.; Cohen, M.; Louie, S. *Phys. Rev. Lett.*, **2011**, *107*, 186404.
- (18) Marques, M. A. L.; Ullrich, C. A.; Nogueira, F.; Rubio, A.; Burke, K.; Gross, E. K. U., *Time-Dependent Density Functional Theory*. Springer: Berlin, Germany, 2006; Vol. 706.
- (19) Runge, E.; Gross, E. K. U. *Phys. Rev. Lett.*, **1984**, *52*, 997-1000.
- (20) Autschbach, J. *ChemPhysChem*, **2009**, *10*, 1757-1760.
- (21) Dreuw, A.; Head-Gordon, M. *J. Am. Chem. Soc.*, **2004**, *126*, 4007-4016.
- (22) Autschbach, J.; Srebro, M. *Acc. Chem. Res.*, **2014**, *47*, 2592-2602.
- (23) Körzdörfer, T.; Brédas, J.-L. *Acc. Chem. Res.*, **2014**, *47* 3284-3291.
- (24) Tozer, D. J. *J. Chem. Phys.*, **2003**, *119*, 12697-12699.
- (25) Yanai, T.; Tew, D. P.; Handy, N. C. *Chem. Phys. Lett.*, **2004**, *393*, 51-57.
- (26) Iikura, H.; Tsuneda, T.; Yanai, T.; Hirao, K. *J. Chem. Phys.*, **2001**, *115*, 3540-3544.
- (27) Sutton, C.; Sears, J. S.; Coropceanu, V.; Brédas, J.-L. *J. Phys. Chem. Lett*, **2013**, *4*, 919-924.
- (28) Fonari, A.; Sutton, C.; Brédas, J.-L.; Coropceanu, V. *Phys. Rev. B*, **2014**, *90*, 165205.
- (29) Sun, H.; Autschbach, J. *ChemPhysChem*, **2013**, *14*, 2450-2461.
- (30) Savin, A., On degeneracy, near-degeneracy and density functional theory. In *Recent Developments and Applications of Modern Density Functional Theory*, Seminario, J. M., Ed.; Elsevier: Amsterdam, 1996; Vol. 4, pp 327-357.
- (31) Salzner, U.; Aydin, A. *J. Chem. Theory Comput*, **2011**, *7*, 2568-2583.
- (32) Stein, T.; Kronik, L.; Baer, R. *J. Am. Chem. Soc.*, **2009**, *131*, 2818-2820.
- (33) Körzdörfer, T.; Sears, J. S.; Sutton, C.; Brédas, J.-L. *J. Chem. Phys.*, **2011**, *135*, 204107-6.
- (34) Sun, H.; Autschbach, J. *J. Chem. Theory Comput.*, **2014**, *10*, 1035-1047.
- (35) Stein, T.; Eisenberg, H.; Kronik, L.; Baer, R. *Phys. Rev. Lett.*, **2010**, *105*, 266802.
- (36) Baer, R.; Livshits, E.; Salzner, U. *Annu. Rev. Phys. Chem.*, **2010**, *61*, 85-109.
- (37) Levy, M.; Perdew, J. P.; Sahni, V. *Phys. Rev. A*, **1984**, *30*, 2745-2748.
- (38) Kronik, L.; Stein, T.; Refaely-Abramson, S.; Baer, R. *J. Chem. Theory Comput.*, **2012**, *8*, 1515-1531.
- (39) Hirata, S.; Head-Gordon, M. *Chem. Phys. Lett.*, **1999**, *314*, 291-299.
- (40) Peach, M. J. G.; Williamson, M. J.; Tozer, D. J. *J. Chem. Theory Comput.*, **2011**, *7*, 3578-3585.
- (41) Peach, M. J. G.; Tozer, D. J. *J. Phys. Chem. A*, **2012**, *116*, 9783-9789.
- (42) Chantzis, A.; Laurent, A. D.; Adamo, C.; Jacquemin, D. *J. Chem. Theory Comput.*, **2013**, *9*, 4517-4525.
- (43) Moral, M.; Muccioli, L.; Son, W. J.; Olivier, Y.; Sancho-García, J. C. *J. Chem. Theory Comput.*, **2015**, *11*, 168-177.

- 1
2
3
4 (44) Frisch, M. J.; Trucks, G. W.; Schlegel, H. B.; Scuseria, G. E.; Robb, M. A.; Cheeseman,
5 J. R.; Scalmani, G.; Barone, V.; Mennucci, B.; Petersson, G. A.; Nakatsuji, H.; Caricato, M.; Li,
6 X.; Hratchian, H. P.; Izmaylov, A. F.; Bloino, J.; Zheng, G.; Sonnenberg, J. L.; Hada, M.; Ehara,
7 M.; Toyota, K.; Fukuda, R.; Hasegawa, J.; Ishida, M.; Nakajima, T.; Honda, Y.; Kitao, O.;
8 Nakai, H.; Vreven, T.; Montgomery Jr., J. A.; Peralta, J. E.; Ogliaro, F.; Bearpark, M. J.; Heyd,
9 J.; Brothers, E. N.; Kudin, K. N.; Staroverov, V. N.; Kobayashi, R.; Normand, J.; Raghavachari,
10 K.; Rendell, A. P.; Burant, J. C.; Iyengar, S. S.; Tomasi, J.; Cossi, M.; Rega, N.; Millam, N. J.;
11 Klene, M.; Knox, J. E.; Cross, J. B.; Bakken, V.; Adamo, C.; Jaramillo, J.; Gomperts, R.;
12 Stratmann, R. E.; Yazyev, O.; Austin, A. J.; Cammi, R.; Pomelli, C.; Ochterski, J. W.; Martin, R.
13 L.; Morokuma, K.; Zakrzewski, V. G.; Voth, G. A.; Salvador, P.; Dannenberg, J. J.; Dapprich,
14 S.; Daniels, A. D.; Farkas, Ö.; Foresman, J. B.; Ortiz, J. V.; Cioslowski, J.; Fox, D. J. *Gaussian*
15 *09*, Gaussian, Inc.: Wallingford, CT, USA, 2009.
16 (45) Tomasi, J.; Mennucci, B.; Cammi, R. *Chem. Rev.*, **2005**, *105*, 2999-3094.
17 (46) Improta, R.; Barone, V.; Scalmani, G.; Frisch, M. J. *J. Chem. Phys.*, **2006**, *125*, 054103.
18 (47) Tamblyn, I.; Refaely-Abramson, S.; Neaton, J. B.; Kronik, L. *J. Phys. Chem. Lett.*, **2014**,
19 *5*, 2734-2741.
20 (48) Perdew, J. P.; Schmidt, K. *AIP Conf. Proc.*, **2001**, *577*, 1-20.
21 (49) Perdew, J. P.; Burke, K.; Ernzerhof, M. *Phys. Rev. Lett.*, **1996**, *77*, 3865-3868.
22 (50) Becke, A. D. *J. Chem. Phys.*, **1993**, *98*, 5648-5652.
23 (51) Lee, C.; Yang, W.; Parr, R. G. *Phys. Rev. B*, **1988**, *37*, 785-789.
24 (52) Zhao, Y.; Truhlar, D. G. *Theor. Chem. Acc.*, **2008**, *120*, 215-241.
25 (53) Zhao, Y.; Truhlar, D. G. *J. Phys. Chem. A*, **2006**, *110*, 13126-13130.
26 (54) Vydrov, O. A.; Scuseria, G. E. *J. Chem. Phys.*, **2006**, *125*, 234109.
27 (55) Chai, J.-D.; Head-Gordon, M. *J. Chem. Phys.*, **2008**, *128*, 084106.
28 (56) Jacquemin, D.; Perpète, E. A.; Ciofini, I.; Adamo, C. *J. Chem. Theory Comput.*, **2010**, *6*,
29 1532-1537.
30 (57) Beljonne, D.; Shuai, Z.; Friend, R. H.; Brédas, J. L. *J. Chem. Phys.*, **1995**, *102*, 2042-
31 2049.
32 (58) Beljonne, D.; Cornil, J.; Friend, R. H.; Janssen, R. A. J.; Brédas, J. L. *J. Am. Chem. Soc.*,
33 **1996**, *118*, 6453-6461.
34 (59) Cohen, A. J.; Mori-Sánchez, P.; Yang, W. *Science*, **2008**, *321*, 792-794.
35 (60) Körzdörfer, T.; Parrish, R. M.; Marom, N.; Sears, J. S.; Sherrill, C. D.; Brédas, J.-L.
36 *Phys. Rev. B*, **2012**, *86*, 205110.
37 (61) Valiev, M.; Bylaska, E. J.; Govind, N.; Kowalski, K.; Straatsma, T. P.; Van Dam, H. J. J.;
38 Wang, D.; Nieplocha, J.; Apra, E.; Windus, T. L.; de Jong, W. A. *Comput. Phys. Commun.*,
39 **2010**, *181*, 1477-1489.
40
41
42
43
44
45
46
47
48
49
50
51
52
53
54
55
56
57
58
59
60

TOC

